Applied Catalysis B: Environmental 330 (2023) 122592

Contents lists available at ScienceDirect

Applied Catalysis B: Environmental

journal homepage: www.elsevier.com/locate/apcatb

Ligand-assisted heterogeneous catalytic H_2O_2 activation for pollutant degradation: The trade-off between coordination site passivation and adjacent site activation

Qing-Qing Huang [a,1], Hong-Zhi Liu [b,1], Mingjie Huang [b,c,*], Jin Wang [a], Han-Qing Yu [b,**]

[a] School of Resources and Environmental Engineering, Hefei University of Technology, Hefei 230026, China
[b] CAS Key Laboratory of Urban Pollutant Conversion, Department of Environmental Science and Engineering, University of Science and Technology of China, Hefei 230026, China
[c] School of Environmental Science and Engineering, Huazhong University of Science and Technology, Wuhan 430074, China

ARTICLE INFO

Keywords:
Ligand
Heterogeneous Fenton reaction
$BiFeO_3$
Electronic modification
Active site identification

ABSTRACT

Ligand modification is an effective and universal strategy to enhance the sluggish surface reaction kinetic in the heterogeneous Fenton system. However, the mechanistic for the promotion effect concerning the complex surface adsorption/activation processes remains unrevealed. Herein, we find that the catalytic H_2O_2 activation ability of $BiFeO_3$ can be significantly enhanced by EDTA and other polycarboxylate ligands. The complexing effect of EDTA enhances the activation rate of H_2O_2 via decreasing the redox potential of the Fe^{III}/Fe^{II} pair, also remarkably improves the utilization efficiency of H_2O_2 via preserving the electron-rich Fe^{II} under the attack of $O_2^{\bullet-}/HO_2^{\bullet}$. More importantly, based on kinetic analyses and theoretical calculations, we reveal that the active site for H_2O_2 activation on the EDTA-adsorbed $BiFeO_3$ surface is the adjacent free Fe^{III}, rather than the EDTA complexing Fe^{III} and the non-adjacent free Fe^{III}. A unique dual effect mechanism of EDTA on the heterogeneous Fenton reaction via the coordination site passivation and adjacent site activation is elucidated. This work clarifies the microcosmic role of ligands in governing the catalytic activity of the surface active site, also provide a significant guidance to rationally develop efficient ligand-assisted heterogeneous reaction system for pollutant degradation.

1. Introduction

Fenton reaction, as a typical advanced oxidation process (AOP), has attracted increasing interests for water pollution control [1,2]. The key reaction of such a process is the activation of hydrogen peroxide (H_2O_2) through the redox cycle of the dissolved Fe^{2+}/Fe^{3+} species to form •OH, which possesses an ultrahigh redox potential ($E_0 = 1.89–2.72$ V vs. NHE) and can non-selectively degrade most of the refractory organic pollutants at near diffusion-limited rates [3–6]. However, the Fe^{2+}/Fe^{3+}-based homogeneous Fenton reaction suffers from several major drawbacks in applications, such as the narrow working pH range (2−4) and the production of a large amount of the iron sludge [7,8]. To address these challenges, heterogeneous Fenton-like process based on the iron oxides (Fe_xO_y) has therefore been extensively pursued as an alternative to the homogeneous one [9,10]. The elaborately designed solid catalysts avoid the need for large amounts of reducing Fe^{2+} ions, also can be readily recycled after the degradation reaction, which has been a hot research topic recently [11–14]. However, the intrinsic insufficient coordination bond and the low abundance of the surface-active sites endorse the Fe_xO_y with a low Fenton-like catalytic ability [4], and it is highly desirable to develop effective enhancement strategy to boost the activity of the relatively inert surface metal sites.

In a typical Fenton reaction process, H_2O_2 is decomposed into •OH by the cycle involving the Fe^{3+} and Fe^{2+} ions. The overall reaction rate is limited by the reduction of Fe^{3+} to Fe^{2+} by oxidizing H_2O_2 [15,16]. For instance, the second-order reaction constant for Fe^{2+} oxidation ($k = 63$ M^{1-} s^{-1}) is 4–5 orders of multitude higher than that of the Fe^{3+} reduction ($k = 0.002–0.01$ $M^{-1}s^{-1}$) [17,18]. In order to promote the

* Corresponding author at: CAS Key Laboratory of Urban Pollutant Conversion, Department of Environmental Science and Engineering, University of Science and Technology of China, Hefei 230026, China.
** Corresponding author.
E-mail addresses: mingjiehuang@hust.edu.cn (M. Huang), hqyu@ustc.edu.cn (H.-Q. Yu).
[1] These authors contributed equally to this work.

https://doi.org/10.1016/j.apcatb.2023.122592
Received 30 December 2022; Received in revised form 21 February 2023; Accepted 6 March 2023
Available online 7 March 2023

efficiency of the Fenton process, ligands were often adopted to enhance the Fe^{3+}/Fe^{2+} cycle by decreasing the redox potential of the Fe^{3+}/Fe^{2+} pair [18,19]. It was reported that the complexation of N,N-bis (carboxymethyl)glutamic acid (GLDA) greatly reduced the potential value of Fe^{3+}/Fe^{2+} from 0.77 V to 0.185 V, thus enhancing the degradation kinetic of ciprofloxacin by nearly 14 times [20]. Similarly, ligands were also employed to enhance the heterogeneous Fenton reaction efficiency. For example, dosing EDTA into the H_2O_2-$BiFeO_3$ system significantly increased the bisphenol A removal from 20.4 % to 91.2 % [21]. But differing from the above concise and explicit homogeneous reaction system, the promotion mechanism of ligand for heterogeneous Fenton reaction regarding the complex surface adsorption and activation processes remains unclear.

Ligands can change the coordination environment of the active site via surface complexation, it can also promote the detachment of the metal ions via the complexing dissolution [22,23]. Thus, the reactions occurring in both the solid-liquid interface and the bulk solution can be affected by the ligands. The ligand-enhancement effect for the bulk solution reaction can be well-established by evaluating the contribution of the leached metal ions [24,25]. However, due to the complex and elusive feature of the microscopic interface, the role of ligands in affecting the surface reaction is still ambiguous. EDTA was reported to enhance the Fenton-like catalytic ability of $BiFeO_3$ via forming a cave on its surface, thus resulting in a higher local concentration of H_2O_2 for Fenton reaction than the bared $BiFeO_3$ surface [21,26]. EDTA was also reported to hinder the heterogeneous Fenton reaction via competing for the surface active sites with organic compounds and H_2O_2 [27]. Thus, the ligand-enhanced heterogeneous Fenton reaction mechanism remains unrevealed and a mechanistic study from the molecular aspect is needed to fully address the above contradictory interpretations.

In this work, the ligand-enhancement mechanism for heterogeneous Fenton reaction in the $BiFeO_3/H_2O_2$ system was investigated. The physicochemical properties and the Fenton-like catalytic features of $BiFeO_3$ synthesized by a sol-gel method were fully examined. By a combination of kinetic analyses, characterizations, electrochemical tests, and density functional theory (DFT) calculations, a unique dual effect mechanism of EDTA on the heterogeneous Fenton reaction via the coordination site passivation and adjacent site activation for pollutants degradation was elucidated. The findings of this work not only give new insights into the ubiquitous ligand-participated surface Fenton catalytic reaction mechanisms for water purification, but also provide fundamental guidance for other processes with great environmental significance, such as removal of emerging contaminants, understanding of organic pollutants in geochemical processes, and production of high value-added chemicals.

2. Materials and methods

2.1. Materials

$Bi(NO_3)_3$•5 H_2O, 2-methoxyethanol, hydrogen peroxide (H_2O_2, 30 wt%), terephthalic acid, 2-hydroxyterephthalic acid, potassium titanium oxide dihydrate, Nafion reagent, and 5,5-Dimethyl-1-pyridine-n-oxide (DMPO) were purchased from Sigma-Aldrich, China. $Fe(NO_3)_3$•9 H_2O, phenol, methanol (MA), ethanol (EA), ethylene glycol, citric acid, disodium ethylenediaminetetraacetate (EDTA), sodium oxalate (OX), nitrilotriacetic acid (NTA), and diethylenetriaminepentaacetic acid (DTPA) were purchased from Shanghai Chemical Reagent Co., China. All chemicals and reagents were of analytical grade and ultrapure water was used throughout the experiments.

2.2. Catalyst synthesis

$BiFeO_3$ nanoparticles were synthesized by a sol-gel method [28]. Ca. 5 mM (2.425 g) $Bi(NO_3)_3$•5 H_2O and 5 mM (2.02 g) $Fe(NO_3)_3$•9 H_2O were firstly added into 24 mL 2-methoxyethanol, then the mixture was ultrasonically dissolved to obtain a transparent solution. Thereafter, ca. 10 mM (2.1 g) citric acid as a complexant and 12 mL of ethylene glycol as a dispersant were added. The mixture was stirred for 1 h at room temperature before being transferred to a 50 mL ceramic crucible, which was heated in an oven at 120 °C for 12 h to form the dry gel. The obtained gel was finally calcined at 500 °C for 2 h to give the $BiFeO_3$ nanoparticles, which was fully ground, washed 3 times with pure water and dried at 60 °C for further use.

2.3. Characterizations

The morphological features of the $BiFeO_3$ nanoparticles were characterized by a field scanning electron microscopy (FESEM) (SU8220, Hitachi Co., Japan) and transmission electron microscopy (TEM) (H7650, Hitachi Co., Japan) equipped with an energy dispersive X-ray energy spectroscopy (EDX). The BET surface area with N_2 adsorption/desorption isotherm was obtained by an ASAP2460 analyzer (Micromeritics Inc., USA). The X-ray diffraction (XRD) pattern of the sample in the range 10–70° was recorded using a Philips X′Pert PRO diffractometer with graphite monochromated Cu Kα radiation ($\lambda = 0.15406$ nm). The surface states of the catalyst and their chemical shifts were determined using an X-ray photoelectron spectroscopy (XPS, ESCALAB250, Thermo Fisher Inc., USA), and the binding energies of all peaks were referenced to the C 1s line (284.8 eV).

2.4. Phenol degradation tests

Phenol degradation tests were conducted at least in duplicate in 250 mL beakers at 25 °C under magnetic stirring. In a typical test, a certain mass of $BiFeO_3$ particles was ultrasonically (ca. 1 min) dispersed into an aqueous solution containing desired amounts of phenol and ligand like EDTA. The degradation reaction was initialed by adding a certain amount of H_2O_2. Before the reaction, the initial pH was adjusted to 4.5 by using 0.5 mM H_2SO_4 or NaOH. The scavenging experiments were conducted with the pre-addition of EA into the reaction system. In the reaction process, approximately 1 mL of reaction suspension was withdrawn and quenched by excess EA, then filtered immediately through a 0.22-μm membrane for organic analysis.

2.5. Analyses

Electron paramagnetic resonance spectroscopy (EPR, EMX, Bruker Co., Germany) measurements were performed using DMPO as a spin trap to detect the radical species. Phenol concentration was detected by a high-performance liquid chromatography (LC-15 C, Shimadzu Co., Japan) system equipped with a C18 column (4.6 25 cm) with UV detector. The mobile phase was a mixture of acetonitrile/formic acid (0.1 %, v/v) (40:60, v/v) at a flow rate of 0.4 mL/min with a UV detector at 273 nm·H_2O_2 concentration was spectroscopically measured by a UV-Vis spectrophotometer (UV-2600, Shimadzu Co., Japan) using the potassium titanium bisoxalate chromogenic method at 420 nm [29,30]. The concentration of •OH was detected by using the terephthalic acid probing method, 2-hydroxy terephthalic acid as the fluorescent oxidation product was quantified by a fluorescence spectrophotometer at an excitation wavelength of 320 nm [31]. The chronoamperometry tests were conducted on a standard three-electrode system (CHI 760E, Chenhua Co., China) to monitor the effects of different ligands (e.g., EDTA, NTA, DTPA, and OX) on the electron transfer process between $BiFeO_3$ and H_2O_2. In such an electrochemical test, platinum wire and saturated Ag/AgCl electrode were selected as the counter and reference electrode, respectively. For the working electrode preparation, ca. 10 mg $BiFeO_3$ was first added into a mixture consisting of 0.75 mL ethanol and 0.05 mL Nafion. The mixture was ultrasonically treated for 30 min to obtain a uniform-dispersed suspension, ca. 0.1 mL of the resultant suspension was dropped onto a carbon paper and dried for several minutes in a far-infrared dryer; this procedure was repeated for four times

to uniformly load enough of the $BiFeO_3$ nanoparticles on the carbon paper. In a chronoamperometric measurement, the working electrode was biased at an applied potential of the open circuit voltage. The current change was monitored immediately after the successive addition of different concentrations of ligands (ca. 0, 0.5, 1, 2, and 4 mM) and H_2O_2 (ca. 10 mM) at the reaction times of 200 s and 400 s, respectively. The in situ attenuated total reflection FTIR (ATR-FTIR) spectra were recorded on a Vertex 70 spectrometer (Bruker Co., Germany) equipped with an external liquid-nitrogen-cooled mercury cadmium telluride detector. A spectrum of a $BiFeO_3$-decorated ZnSe crystal window was collected as the background. The EDTA solution as subsequently added and monitored by the FTIR spectroscopy, and 64 scans were collected at a 2 cm^{-1} resolution every 2 min

2.6. Calculations

DFT calculations involving geometry optimization, energy calculations, and charge density difference were performed using the CASTEP package of Material Studio. The generalized gradient approximation (GGA) and the Perdew-Burke-Ernzerhof (PBE) functional were used to describe the exchange-correlation interaction [32]. In geometry optimization, until the energy was less than 1×10^{-5} eV/atom, the structure tended to be stable and the energy reached a minimum. The surface atoms were fully relaxed until the maximum force, maximum stress, and maximum displacement per atom were less than 0.03 eV/Å, 0.05 GPa, 1×10^{-3} Å, respectively, while the underlying atoms were constrained. During electron minimization optimization, The OTFG supersoft pseudopotential was used with the energy cutoff of 571.4 eV and a *k*-point set of $1 \times 1 \times 1$. The self-consistent field (SCF) tolerance was set to 1×10^{-6} eV/atom for geometric and electronic optimization.

The original $BiFeO_3$ model adopted the *R3c* structure with lattice constants a = 5.588 Å, b = 5.588 Å, c = 13.867 Å, included angles $\alpha = \beta = 90°$, $\gamma = 120°$. To expose Fe and Bi atoms on the surface at the same time, the (111) crystal plane was chosen as the research object. Then, a periodic 2×3 supercell with a total of 120 atoms was built, including 24 iron atoms, 24 bismuth atoms, 72 oxygen atoms, and a vacuum layer of 15 Å in the *z*-orientation was set. For a more negative adsorption energy (ΔE_{ad}, eV), a more stable structure is used. The adsorption energies of EDTA and H_2O_2 on the $BiFeO_3$(111) surface, and H_2O_2 on the EDTA-absorbed $BiFeO_3$(111) surface are denoted as ΔE_{ad1}, ΔE_{ad2}, and ΔE_{ad3}, respectively, which are calculated with the following equations:

$$\Delta E_{ad1} = E_{EDTA+BiFeO3} - E_{EDTA} - E_{BiFeO3} \quad (1)$$

$$\Delta E_{ad2} = E_{H2O2+BiFeO3} - E_{H2O2} - E_{BiFeO3} \quad (2)$$

$$\Delta E_{ad3} = E_{EDTA+H2O2+BiFeO3} - E_{EDTA} - E_{H2O2} - E_{BiFeO3} \quad (3)$$

To further examine the effect of EDTA coordination on $BiFeO_3$, the charge density difference and Mulliken charge analysis were carried out from a perspective of electron transfer, and the reaction energy analysis was carried out from a perspective of energy.

3. Results and discussion

3.1. Physicochemical properties of the $BiFeO_3$ catalyst

The crystalline structure of the synthesized $BiFeO_3$ nanoparticles was characterized by the XRD analysis. As shown in Fig. 1a, the sharp diffraction peaks of the sample were identical to those of $BiFeO_3$ perovskite (Joint Committee Powder Diffraction Standards No. 86–1518), indicating the successful synthesis of the well-crystalline and high-purity $BiFeO_3$ catalyst. The N_2 adsorption-desorption isotherm in Fig. 1b displayed a gradual curvature feature, which corresponded to the typical III-type characteristic, indicating the absence of mesoporous structure (2–50 nm) of the synthesized $BiFeO_3$ catalyst [33]. The BET surface area and the average pore size were measured to be 6.67 m^2/g and 17.83 nm, respectively. In addition, the SEM images in Fig. 1c clearly show the aggregation of the individual $BiFeO_3$ nanosphere, which had an average size of ~100 nm as depicted in the TEM image (Fig. 1d). The high-resolution TEM (HR-TEM) pattern in Fig. 1e displays

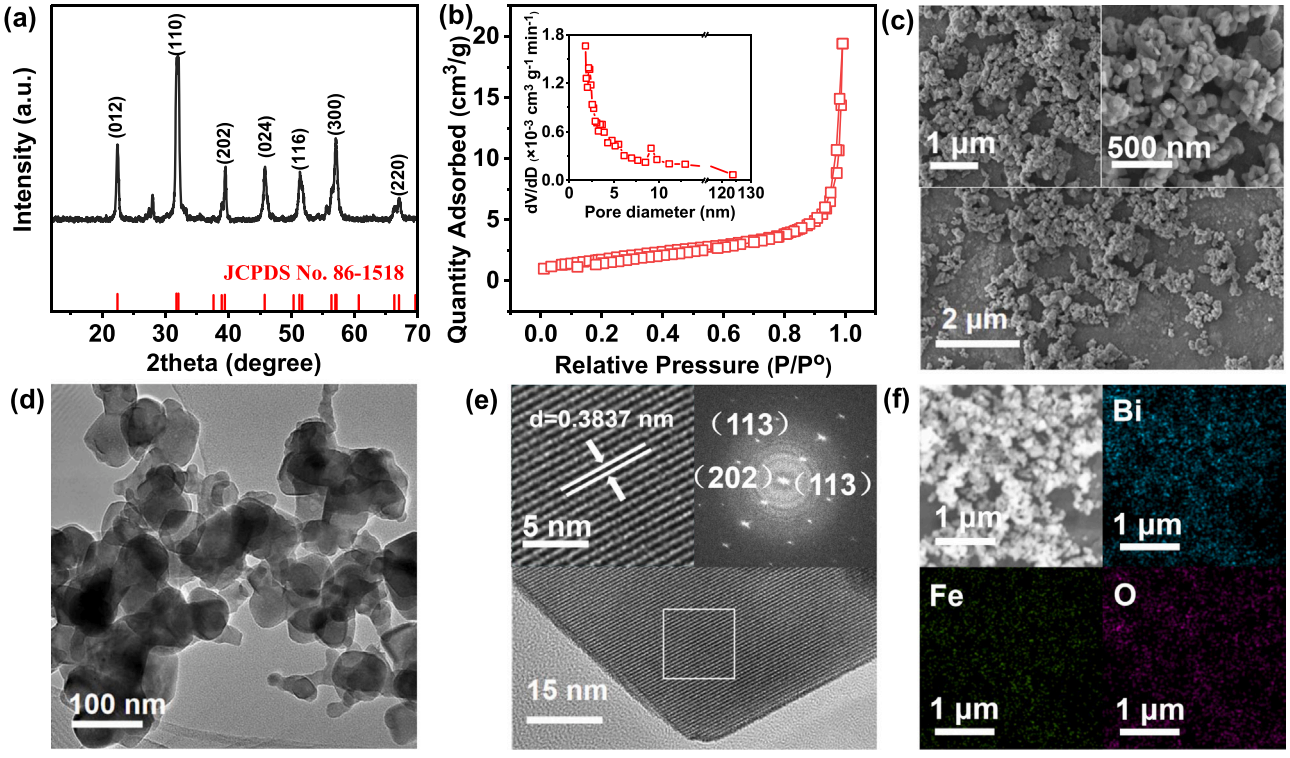

Fig. 1. Characteristics of the $BiFeO_3$ catalyst. (a) XRD pattern, (b) N_2 adsorption-desorption isotherm, (c) SEM, (d) TEM, (e) HRTEM, and (f) TEM-EDS mapping images of the $BiFeO_3$ catalyst.

a well-defined lattice structure of the $BiFeO_3$ catalyst with the lattice spacing of 0.384 nm corresponding to the $BiFeO_3$ (100) facet [34]. These results further confirm the pure crystalline structure of the sample. Furthermore, the TEM-EDS element mapping images (Fig. 1f) display that the Bi, Fe, and O elements were homogeneously distributed over the nanospheres.

3.2. Enhanced phenol degradation by EDTA in the Fenton-like system

The enhancement effect of EDTA for heterogeneous Fenton-like reaction was demonstrated for the rather rapider phenol degradation compared to the control reaction system without ligand addition. As shown in Fig. 2, in 45-min reaction process approximately 68.7% of phenol was degraded in the $BiFeO_3/H_2O_2$/EDTA system, while it was only 23.9% in the absence of EDTA. In such two reaction systems, the degradation of phenol could be well fitted by the pseudo-first order kinetic model, with the reaction constant (k_{obs}) calculated to be 2.5 and 0.63 min^{-1}, respectively. Besides, negligible phenol was removed via the $BiFeO_3$ adsorption. These results demonstrate the critical role of EDTA in enhancing phenol degradation in the $BiFeO_3$-based Fenton-like reaction system. In addition, the leached Fe and Bi ions concentration were measured to be 0.6 and 20.9 mg/L, which had no contribution to phenol degradation in the presence of EDTA (Fig. S1). The negligible resonant absorption in the low-field resonance part indicated the absence of oxygen vacancy of the $BiFeO_3$ catalyst (Fig. S2). These results indicate that the obviously improved phenol degradation in the $BiFeO_3/H_2O_2$/EDTA system could be attributed to the surface atomic/electronic modification of $BiFeO_3$ by EDTA.

The effect of critical parameters, e.g., $BiFeO_3$ dosage, H_2O_2, phenol, and EDTA concentrations, on phenol degradation was then examined. As shown in Fig. S3a, as the initial $BiFeO_3$ dosage was increased from 0.25 to 2 g/L, the phenol degradation efficiency significantly increased from 54.3 % to 89.7 %. However, a further increase in $BiFeO_3$ dosage led to an obvious decrease to 69.3 %, which could be attributed to the scavenging effect of the $BiFeO_3$ catalyst [35]. Generally, the amount of generated reactive oxygen species (ROS, e.g., •OH) directly relates to the H_2O_2 concentration. As shown in Fig. S3b, the phenol decomposition rate was drastically accelerated when increasing the H_2O_2 concentration from 2.5 to 30 mM. Besides, as the phenol concentration was increased from 5 to 45 μM, the apparent degradation efficiency declined from 89.5 % to 49.1 % due to the competitive effect for the limited ROS between phenol molecules and the deuterogenic by-products (Fig. S3c). In addition, EDTA as the critical additive showed a great promotion effect on phenol degradation with an initial concentration from 0.05 to 1.0 mM, while the phenol degradation rate was obviously hindered when the EDTA concentration was further increased to 2.0 mM (Fig. S3d). Apart from the explicit reason that excess EDTA can compete with phenol for the limited ROS, another important factor also involves, that is, the modified surface atomic structure with overloaded EDTA is unfavorable for H_2O_2 activation [36]. Such a conclusion can be further evidenced by the obviously different responses for phenol degradation to the pH changes with or without EDTA addition (Figs. S4 and S5). These results show that the phenol degradation efficiency displayed a monotonic decease with the pH value, this is consistent with the expectation because a higher pH can inhibit the dissolution of Fe ions and the homogeneous Fenton reaction. While in stark contrast, the phenol degradation efficiency exhibited a volcanic trend with the increasing pH in the presence of EDTA. An optimal reaction pH was obtained at 4.5, both the acidic and alkaline conditions hindered the phenol degradation. This result indicates that the moderate coverage of EDTA on the surface of $BiFeO_3$ was beneficial to H_2O_2 activation and phenol degradation.

3.3. Mechanism for the enhancement effect of EDTA

EDTA could greatly enhance the phenol degradation via $BiFeO_3$ surface atomic structure modification. Such an enhancement could be attributed to the significantly elevated •OH production as proven by the qualitative and quantitative experiments of the involved reactive species. Since the interfacial complexation of EDTA cannot be affected by the co-existed ethanol (Figs. S6 and S7), the main reactive species for phenol degradation with or without EDTA addition were firstly explored by the ethanol scavenging experiments (Fig. 3a). The results show that methanol, as a •OH quencher ($k = 9.7 \times 10^8$), completely inhibited the degradation of phenol in both $BiFeO_3/H_2O_2$ and $BiFeO_3/H_2O_2$/EDTA systems, indicating the similar •OH-dominant degradation mechanism in the two systems [35,37]. Besides, the EPR experiments using DMPO as the trapping agent showed distinct quartet peaks with an intensity ratio of 1:2:2:1 (Fig. 3b), corresponding to the occurrence of •OH [38,39]. Obviously, the peak intensity of •OH was significantly enhanced after dosing EDTA, further validating the critical role of EDTA in promoting •OH generation and phenol degradation. These results also indicate that EDTA accelerated the degradation of phenol via enhancing the ROS yield, rather than changing its generation pathway.

The substantially higher accumulated •OH concentration in the presence of EDTA was further confirmed by the DMSO quantitative test [40]. The accumulated •OH reached 133.9 μM at 90 min in the $BiFeO_3/H_2O_2$/EDTA system (Fig. 4a), while it was 0.66 μM only in the absence of EDTA. Intriguingly, the decomposition rate of H_2O_2 was even lower in the presence of EDTA, which might be due to the competition

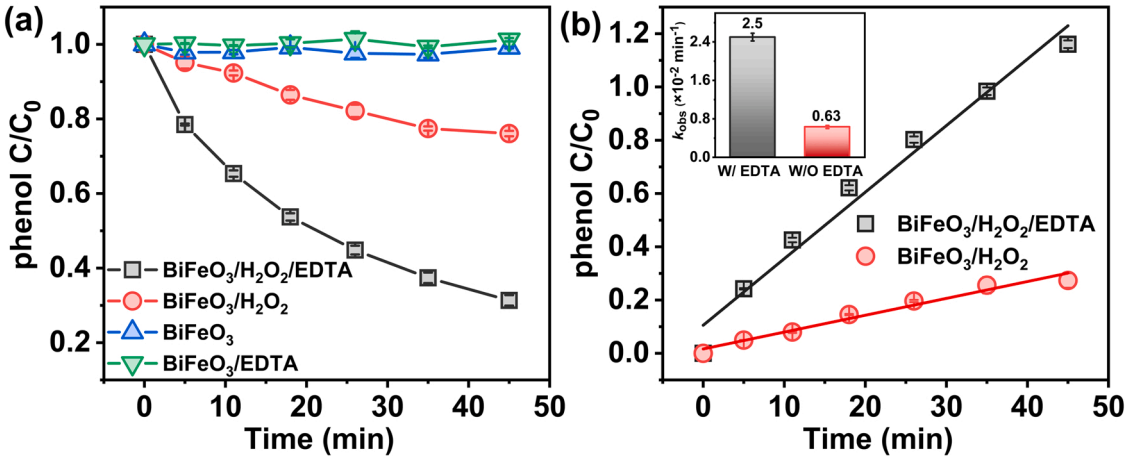

Fig. 2. Degradation of phenol in different reaction systems. (a) The time-dependent evolution of residual phenol concentration, (b) the pseudo-first order reaction kinetic simulation. Experimental conditions: [$BiFeO_3$] = 1 g/L, [H_2O_2] = 10 mM, [phenol] = 0.025 mM, [EDTA] = 1 mM, pH = 4.5, and temperature = 25 ℃.

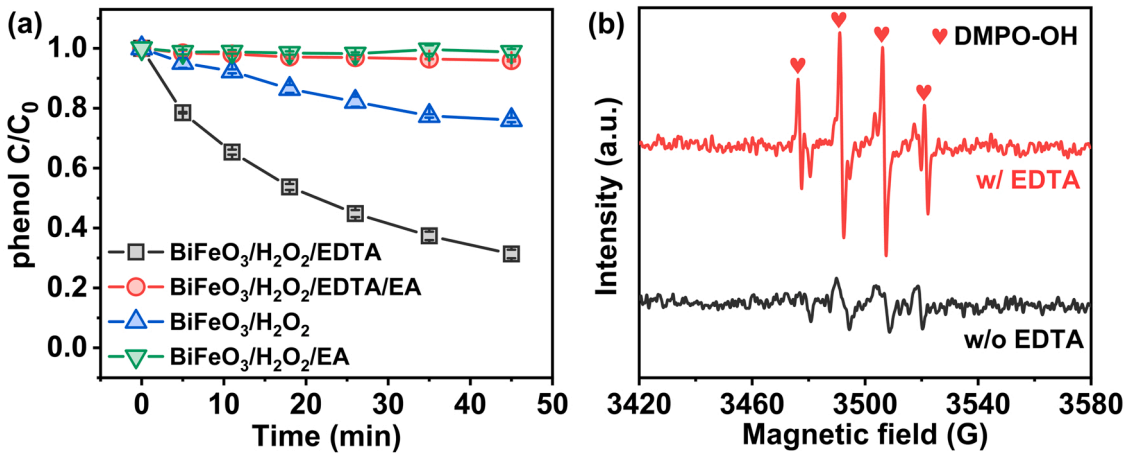

Fig. 3. Reactive species identification. (a) Effect of ethanol on phenol degradation and (b) the EPR spectra for •OH identification in the $BiFeO_3/H_2O_2$/EDTA and $BiFeO_3/H_2O_2$ systems. Experimental conditions: [$BiFeO_3$] = 1 g/L, [H_2O_2] = 10 mM, [phenol] = 0.025 mM, [EDTA] = 1 mM, [DMPO] = 100 mM, [EA] = 500 mM, pH = 4.5, and temperature = 25 °C.

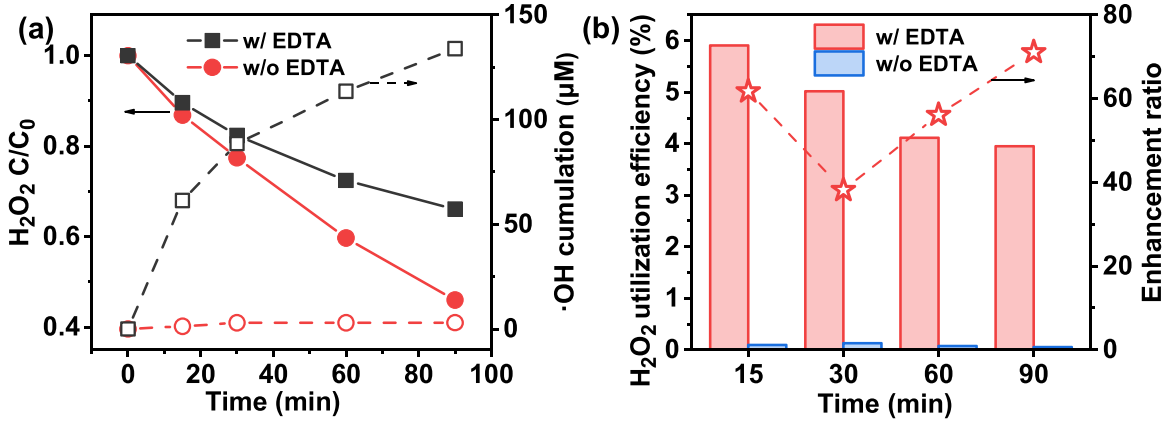

Fig. 4. The utilization efficiency of H_2O_2 in the $BiFeO_3/H_2O_2$/EDTA and $BiFeO_3/H_2O_2$ systems. (a) The decomposition of H_2O_2 and the cumulation of •OH, (b) the utilization efficiency of H_2O_2 and the corresponding enhancement ratio for EDTA at different reaction times. Experimental conditions: [$BiFeO_3$] = 1 g/L, [H_2O_2] = 10 mM, [phenol] = 0.025 mM, [EDTA] = 1 mM, pH = 4.5, and temperature = 25 °C.

effect of EDTA for the surface reactive sites. These results indicate that the enhancement effect of EDTA for •OH production was attributed to its impressive function to elevate the utilization efficiency of H_2O_2. The results in Fig. 4b show that the H_2O_2 utilization efficiency in the $BiFeO_3/H_2O_2$/EDTA system was more than one order of magnitude higher than that in the $BiFeO_3/H_2O_2$ system.

It is interesting to understand why EDTA can significantly promote the utilization efficiency of H_2O_2. We can answer this question by analyzing the two critical steps in H_2O_2 activation, i.e., the reduction of surface Fe^{III} by H_2O_2 to produce Fe^{II} and $HO_2^{\bullet}/O_2^{\bullet-}$ (Eq. 4), and the activation of another H_2O_2 by surface Fe^{II} to produce Fe^{III} and •OH (Eq. 5) [41,42].

$$Fe^{III} + H_2O_2 \rightarrow Fe^{II} + HO_2^{\bullet}/O_2^{\bullet-} + H^+ \; k_1 = 2{\cdot}5\times10^{-3}\ M^{-1}s^{-1} \quad (4)$$

$$Fe^{II} + H_2O_2 \rightarrow Fe^{III} + OH^- + {\bullet}OH \; k_2 = 55\ M^{-1}s^{-1} \quad (5)$$

For the first step (Eq. 4), it is important to clarify the active site for H_2O_2 activation, but whether the EDTA complexing Fe^{III}, the adjacent free Fe^{III}, or the non-adjacent free Fe^{III} (Fig. 5a) are responsible for such process remains unknown. This question can be facilely answered by investigating the relationship between the proportion of these three surface Fe species and the H_2O_2 activation kinetics. Thus, from the qualitative way, the proportion variation tendency of these Fe species along with the EDTA coverage is depicted in Fig. 5b, in which the proportion of the adjacent free Fe^{III} initially increased, but then decreased due to the gradual loading and overloading of EDTA. Then, the effect of EDTA coverage on H_2O_2 activation was examined (Figs. S8 and 5c). It is interesting to note that the decomposition rate of H_2O_2 showed a volcanic-like shape with the increase in EDTA concentration. The results from the homogeneous control experiments and EPR study (Figs. S1 and S2) indicate that the activation process of H_2O_2 occurred heterogeneously on the surface of $BiFeO_3$. The H_2O_2 activation efficiency was thus determined by both the reactivity and quantity of the surface Fe site. The reactivity of the surface Fe site was closely related to its electronic density. Because of the electron-donating ability of EDTA, the reactivity of the surface Fe sites would be higher when EDTA concentration increased. Thus, a decrease in H_2O_2 activation rate at a higher EDTA concentration (Fig. 5c) could be attributed to the decreased Fe site quantity only. The proportion variation tendency of the three Fe species (Fig. 5b) suggests that the adjacent free Fe^{3+} is the active site for H_2O_2 activation. For the left branch of the volcano, an increase in EDTA coverage led to more adjacent free Fe^{III} sites, whereas for the right branch of the volcano, the overloading of EDTA occupied the active site. The optimal EDTA coverage resulted in the highest content of the adjacent free Fe^{III} and thereby led to the superior Fenton activity.

The above conclusion was also verified by the chronoamperometry tests. As shown in Fig. 5d, when EDTA was initially added into the electrochemical system, no electron transfer occurred between EDTA

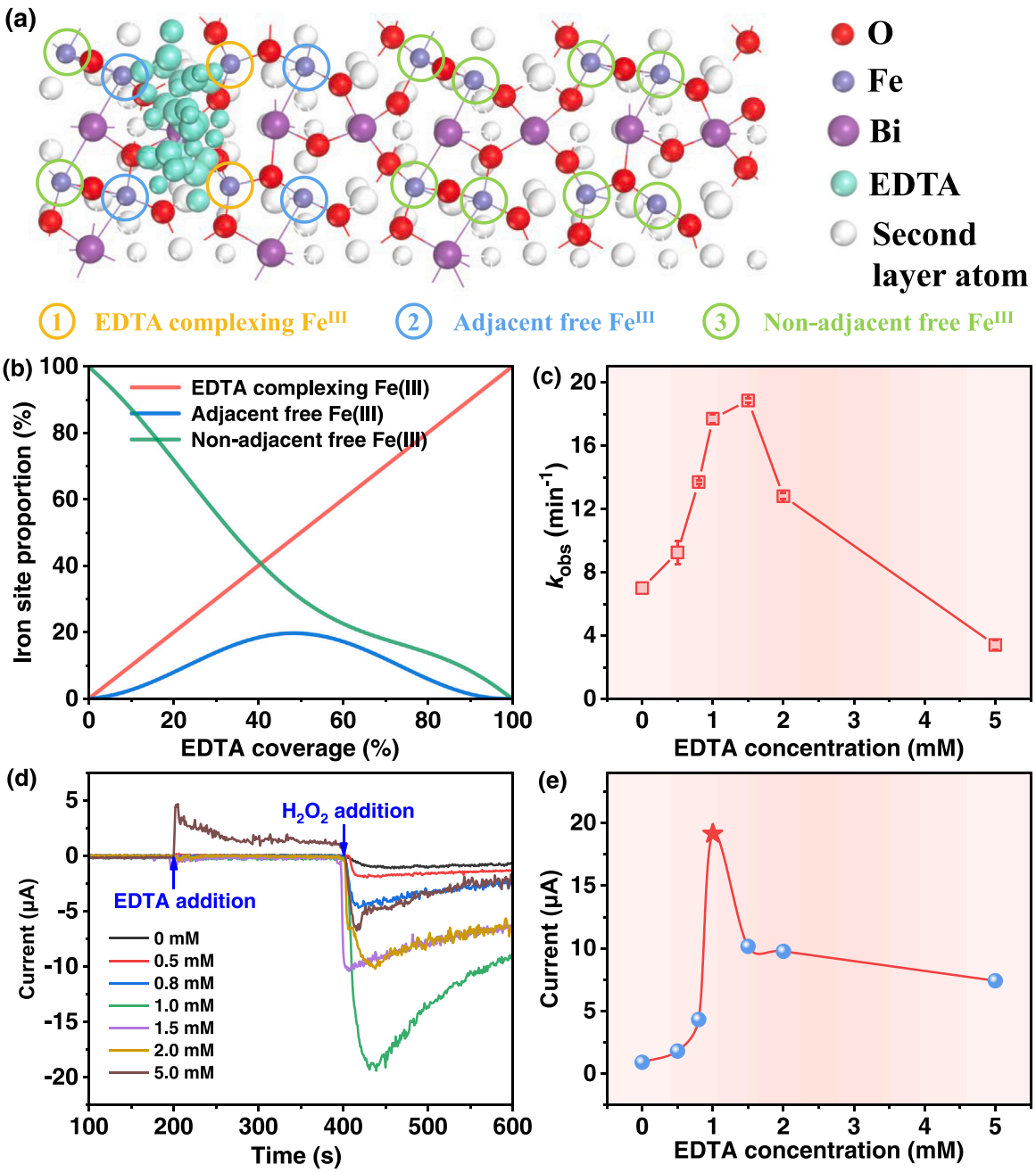

Fig. 5. Identification of the active site for H_2O_2 activation. (a) Illustration of the different iron species on the EDTA-adsorbed $BiFeO_3$ surface, (b) The proportion variation tendency of different Fe species along with the EDTA coverage, (c) the effect of EDTA concentration on the decomposition kinetic of H_2O, (d) chronoamperometry curves after the successive addition of EDTA and H_2O_2, and (e) the effect of EDTA concentration on the response current. Experimental conditions: [$BiFeO_3$] = 1 g/L, [H_2O_2] = 10 mM, pH = 4.5, and temperature = 25 ℃.

and the catalyst, whereas the current output was drastically enhanced when H_2O_2 was subsequently added. Intriguingly, the current intensity between H_2O_2 and $BiFeO_3$ was dependent highly on the EDTA concentration, which also exhibited a volcanic-like shape with the increase in EDTA concentration (Fig. 5e). The optimal EDTA concentration was ca. 1 mM, which was identical to the decomposition kinetic results of H_2O_2 as shown in Fig. 5c, further demonstrating the dual effect of EDTA on H_2O_2 activation via enhancing the generation of the active site (i.e., the adjacent free Fe^{III}) at a low dosage and screening the active site at a high dosage. It is worth noting that the improved H_2O_2 activation rate after EDTA addition was attributed to not only the increased active site content, but also the richer electronic density of the surface active site after EDTA complexing. As shown in Fig. S9, the Fe 2p spectra can be deconvoluted into Fe^{II} (~710.1 eV) and Fe^{III} (~712.5 eV) [43,44]. As the EDTA concentration was increased from 0 to 4 mM, the proportion of surface Fe^{II} substantially increased from 34.9% to 61.2%. The iron center with rich electronic density could deliver a much more rapid reaction constant with H_2O_2 due to the significantly decreased redox potential [45,46].

In addition to EDTA, other polycarboxylic acids such as dicarboxylic acid (e.g., oxalic acid), tricarboxylic acid (e.g., nitrilotriacetic acid, NTA), and pentacarboxylic acid (e.g., diethylenetriaminepentaacetic acid, DTPA) also showed a dual effect on H_2O_2 activation. A similar volcanic-like shape relationship between the ligand concentration and H_2O_2 activation rate was observed (Figs. S10 and 6). These results demonstrate that the organic ligands can induce the generation of the

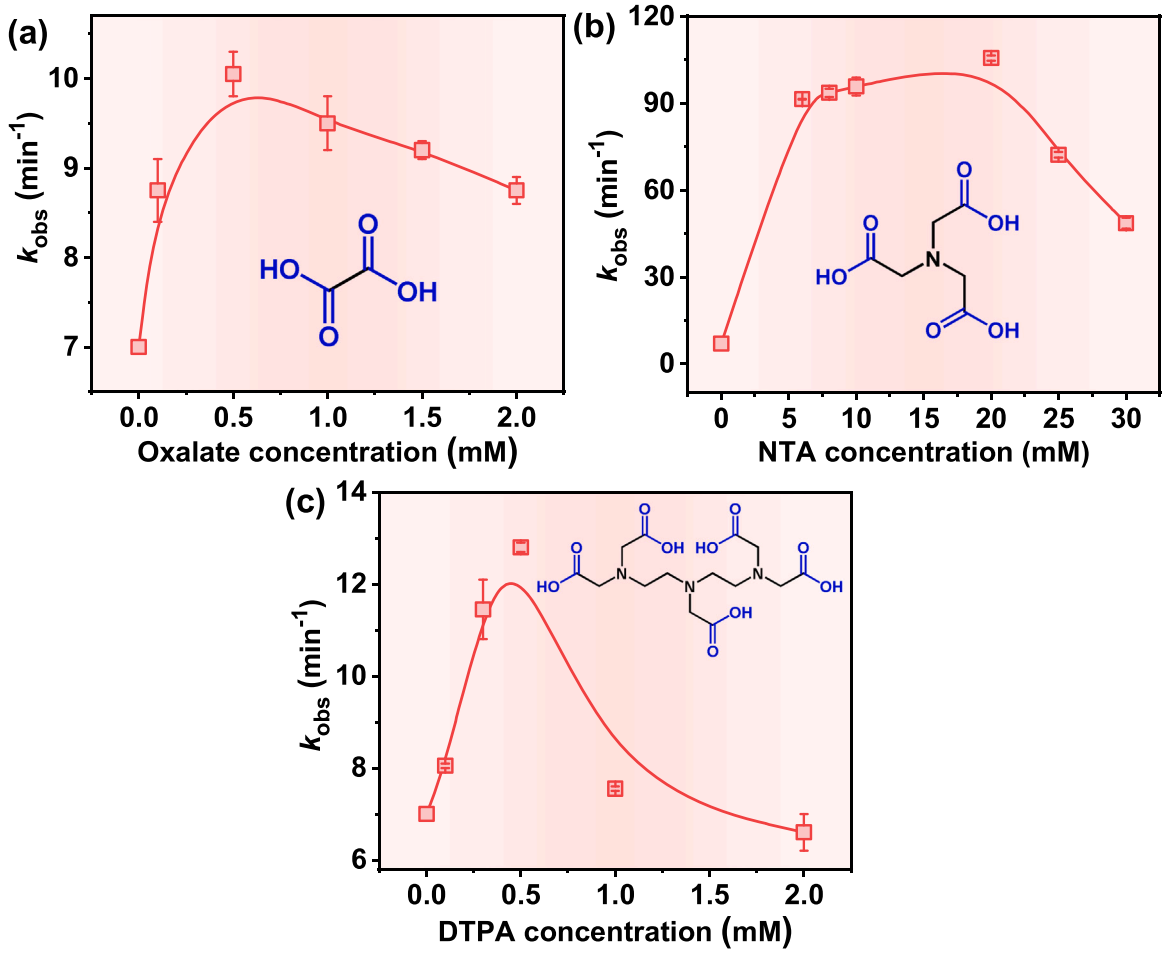

Fig. 6. The effects of different polycarboxylic acids on the H_2O_2 decomposition kinetics. (a) oxalic acid (OA), (d) nitrilotriacetic acid (NTA), and diethylenetriaminepentaacetic acid (DTPA). Experimental conditions: [$BiFeO_3$] = 1 g/L, [H_2O_2] = 10 mM, [OA] = [NTA] = [DTPA] = 1 mM, pH = 4.5, and temperature = 25 °C.

adjacent free Fe^{III} with rich electronic density for enhanced H_2O_2 activation.

For the second step (Eq. 5), a volcanic-like shape for •OH production with the increase in EDTA concentration was also observed. As shown in Figs. S11 and 7a, when the EDTA concentration was increased from 0 to 5 mM, the generation of •OH initially increased, but then decreased. Such a variation trend was similar to that of the H_2O_2 decomposition (Fig. 7b). The increased production of •OH in the left branch of the volcano could be attributed to two factors. The first one was the rapidly accumulated surface Fe^{II} due to EDTA complexing (Eq. 5c and eq. 4). Another was that the Fenton active sites (i.e., Fe^{II}) with higher electronic density can trigger a higher activation rate of H_2O_2 (Eqs. 5–6). Meanwhile, EDTA cannot change the formation rate of $O_2^{\bullet-}$/$HO_2^{\bullet}$ (Eqs. 4 and 7), but lower its consumption rate by one order of multitude (Eqs. 8–11)

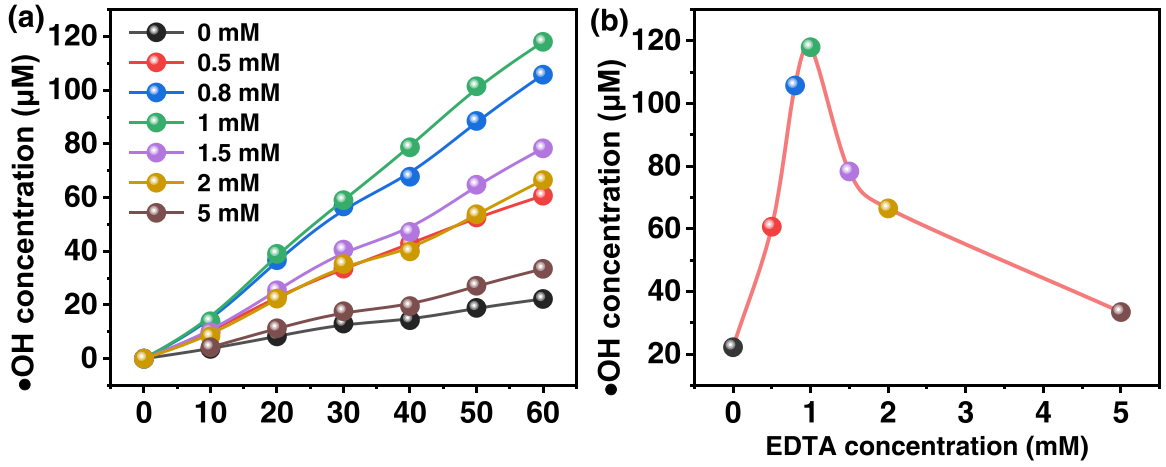

Fig. 7. The effect of EDTA concentration on •OH production. (a) The time-dependent evolution of •OH concentration, (b) the relationship between the EDTA concentration and •OH production. Experimental conditions: [$BiFeO_3$] = 1 g/L, [H_2O_2] = 10 mM, pH = 4.5, and temperature = 25 °C.

[47,48]. Such an inhibitory effect of EDTA could lead to the accumulation of $O_2^{\bullet-}$/$HO_2^{\bullet}$, as verified by the EPR experiments. As shown in Fig. S12, the occurrence of the strong sextet peak was ascribed to the formation of the DMPO-OOH spin adduct, the hyperfine coupling constants were 14.3 G for α_N, 11.4 G for $\alpha_{\beta\text{-H}}$, and 1.2 G for $\alpha_{\gamma\text{-H}}$, validating the generation of $O_2^{\bullet-}$/$HO_2^{\bullet}$ in the $BiFeO_3/H_2O_2$/EDTA system [38]. Obviously, the peak intensity of $O_2^{\bullet-}$/$HO_2^{\bullet}$ was significantly decreased in the system without EDTA addition, indicating that the iron sites with electron-rich feature via EDTA complexing was well-preserved under the attack of $O_2^{\bullet-}$/$HO_2^{\bullet}$, which exhibited an improved Fenton reaction and •OH production rate [21,49].

$$Fe^{II}EDTA + H_2O_2 \rightarrow Fe^{III}EDTA + \bullet OH + OH^- \; k_3 = 2600\ M^{-1}s^{-1} \quad (6)$$

$$Fe^{III}EDTA + H_2O_2 \rightarrow Fe^{II}EDTA + O_2^{\bullet-} + 2\ H^+ \; k_4 = 2{\cdot}5\times10^{-3}\ M^{-1}s^{-1} \quad (7)$$

$$Fe^{II} + O_2^{\bullet-} + 2\ H^+ \rightarrow Fe^{III} + H_2O_2 k_5 = 1\times10^7\ M^{-1}s^{-1} \quad (8)$$

$$Fe^{II}EDTA + O_2^{\bullet-} + 2\ H^+ \rightarrow Fe^{III}EDTA + H_2O_2\ k_6 = 1\times10^6\ M^{-1}s^{-1} \quad (9)$$

$$Fe^{III} + O_2^{\bullet-} \rightarrow Fe^{II} + O_2\ k_7 = 1{\cdot}2\times10^7\ M^{-1}s^{-1} \quad (10)$$

$$Fe^{III}EDTA + O_2^{\bullet-} \rightarrow Fe^{II}EDTA + O_2\ k_8 = 2{\cdot}0\times10^6\ M_1^{-1}{}_s \quad (11)$$

In addition to $BiFeO_3$, other perovskite (e.g., $LaFeO_3$) and spinel (e.g., Fe_3O_4) oxides also exhibited obviously enhanced catalytic phenol degradation in the presence of EDTA. As shown in Fig. S13, the degradation rate of phenol in the $LaFeO_3/H_2O_2$ and Fe_3O_4/H_2O_2 systems were enhanced by 5.0 and 4.7 times by EDTA, indicating the universal functionality of EDTA in enhancing Fenton-like oxidative reactions.

3.4. Mechanism validation by DFT calculations

The promotion mechanism of EDTA for H_2O_2 activation and phenol degradation was further clarified by the DFT calculations. For the first step, the adsorption position and configuration of EDTA on the surface of $BiFeO_3$ were explored. EDTA can be parallelly or perpendicularly adsorbed on different sites of $BiFeO_3$, such as the single Fe site (Fe_1), single Bi site (Bi_1), double Fe sites (Fe-Fe), double Bi sites (Bi-Bi), and Fe-Bi sites (Fe-Bi). Fig. S14 shows the parallelly adsorption configuration of EDTA on the above five adsorption sites of $BiFeO_3$. The negative adsorption energies (ΔE_{ad}) indicate that these adsorption processes were thermodynamically infeasible. By contrast, EDTA can be feasibly adsorbed on the surface of $BiFeO_3$ via the perpendicular configuration, the optimal adsorption site was the double Fe sites (Fe-Fe) with the adsorption energy of − 1.405 eV (Fig. S15). Moreover, Mulliken charge analysis shows that the net charge of adsorbed EDTA was − 1.45, suggesting that 0.55 e^- was transferred from EDTA to $BiFeO_3$ (Fig. S16). The differential charge density analyses (Fig. 8a-b) and the corresponding 2D slice plots (Fig. 8c-d) clearly show the charge accumulation on the Fe atom and the charge depletion on the O atom of EDTA. These results were consistent with the XPS result that EDTA increased the electronic density of the surface Fe on $BiFeO_3$ (Fig. S9). Then, the adsorption of H_2O_2 on the different Fe sites on EDTA-adsorbed $BiFeO_3$ surface was studied (Fig. S17). These three Fe sites were adjacent to the adsorbed EDTA as it was proven that the adjacent free Fe was the active site for H_2O_2 activation (Fig. 5). The results show that H_2O_2 could be spontaneously adsorbed and dissociated on the different Fe sites (Table S1), indicating the promotion effect of EDTA in gaining electronic density of $BiFeO_3$ for enhanced H_2O_2 activation. The critical role of EDTA in promoting H_2O_2 activation was further validated by analyzing the energy change for different activation steps, i.e., the reduction of surface Fe^{III} by H_2O_2 to produce Fe^{II} and $HO_2^{\bullet}/O_2^{\bullet-}$ (Eq. 4), and the activation of H_2O_2 by surface Fe^{II} to produce Fe^{III} and •OH (Eq. 5). As expected, the released energy for the spontaneous H_2O_2 activation to produce •OH significantly increased from 4.650 to 5.691 eV (Fig. 8), indicating that the surface-bound EDTA was highly favorable for H_2O_2 activation.

4. Conclusions

In summary, the heterogeneous Fenton catalytic ability of $BiFeO_3$ could be substantially improved through EDTA modification. The pseudo-first order kinetic constant (k_{obs}) for phenol degradation was 2.5 min^{-1}, which was almost six-fold higher than that for the reaction system without EDTA addition. A combination of batch experiments, characterizations, electrochemical tests, and DFT calculation shows that the active site for H_2O_2 activation on the EDTA-adsorbed $BiFeO_3$ surface was the adjacent free Fe^{III}, rather than the EDTA complexing Fe^{III} and the non-adjacent free Fe^{III}. The promotion mechanism of EDTA can be ascribed two factors. The first one is that EDTA could increase the electronic density of the adjacent free Fe^{III} and decrease the redox potential of the Fe^{III}/Fe^{II} pair, resulting in a higher activation rate of H_2O_2. The second one is that the electron-rich Fe^{II} via EDTA complexing could be well-preserved under the attack of $O_2^{\bullet-}$/$HO_2^{\bullet}$, leading to a significantly improved utilization efficiency of H_2O_2. Therefore, a unique effect mechanism of EDTA on the heterogenous Fenton reaction via the coordination site passivation and adjacent site activation was demonstrated in this work. The results from this work provides new insights

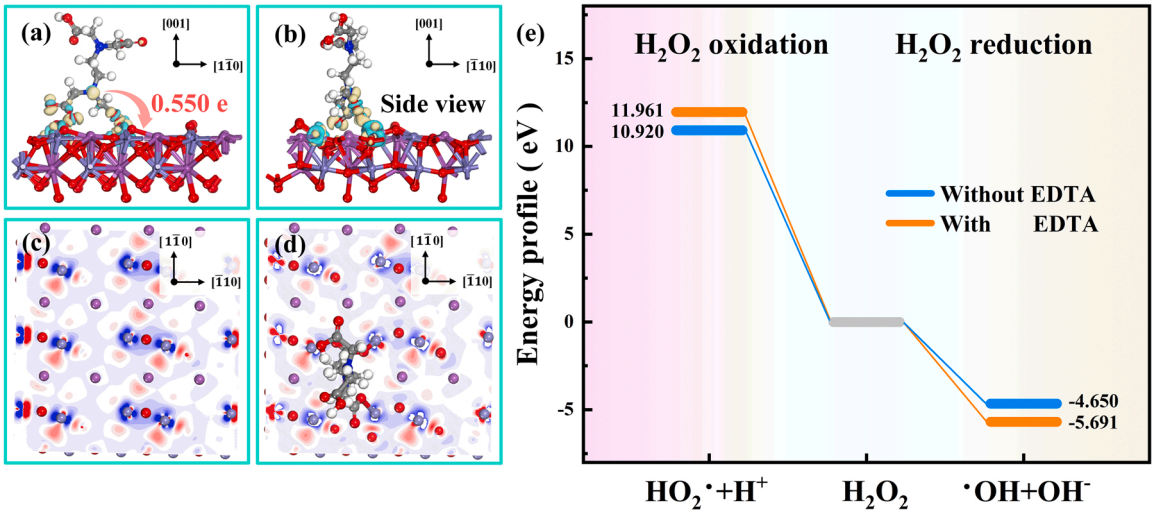

Fig. 8. DFT calculations for understanding the reaction between $BiFeO_3$ and H_2O_2. (a-b) Differential charge density analyses and (c-d) the corresponding 2D slice plots for the EDTA molecule adsorbed on the surface of $BiFeO_3$, (e) free energies for H_2O_2 oxidation and reduction in the presence and absence of EDTA.

into the ubiquitous ligand-participated heterogeneous Fenton reaction systems for catalytic pollutant degradation.

CRediT authorship contribution statement

Qing-Qing Huang: Data curation, Formal analysis, Writing - original draft. **Hong-Zhi Liu:** Software, Computation. **Mingjie Huang:** Conceptualization, Investigation, Supervision, Writing - review & editing. **Jin Wang:** Supervision. **Han-Qing Yu:** Conceptualization, Supervision, Writing - review & editing.

Declaration of Competing Interest

The authors declare that they have no known competing financial interests or personal relationships that could have appeared to influence the work reported in this paper.

Data availability

Data will be made available on request.

Acknowledgments

This work is supported by the National Natural Science Foundation of China (22106159, 52192684 and 51821006). The numerical calculations have been performed on the supercomputing system in the Supercomputing Center of University of Science and Technology of China.

Appendix A. Supporting information

Supplementary data associated with this article can be found in the online version at doi:10.1016/j.apcatb.2023.122592.

References

[1] D.-N. Pei, C. Liu, A.-Y. Zhang, X.-Q. Pan, H.-Q. Yu, In situ organic Fenton-like catalysis triggered by anodic polymeric intermediates for electrochemical water purification, Proc. Natl. Acad. Sci. USA 117 (49) (2020) 30966–30972.
[2] M. Huang, Y.S. Li, C.Q. Zhang, C. Cui, Q.Q. Huang, M. Li, Z. Qiang, T. Zhou, X. Wu, H.Q. Yu, Facilely tuning the intrinsic catalytic sites of the spinel oxide for peroxymonosulfate activation: from fundamental investigation to pilot-scale demonstration, Proc. Natl. Acad. Sci. USA 119 (30) (2022), e2202682119.
[3] J. Wang, X. Dai, H. Wang, H. Liu, J. Rabeah, A. Brückner, F. Shi, M. Gong, X. Yang, Dihydroxyacetone valorization with high atom efficiency via controlling radical oxidation pathways over natural mineral-inspired catalyst, Nat. Commun. 12 (1) (2021) 1–11.
[4] L. Cui, X. Zhao, H. Xie, Z. Zhang, Overcoming the activity-stability trade-off in heterogeneous electro-fenton catalysis: encapsulating carbon cloth-supported iron oxychloride within graphitic layers, ACS Catal. 12 (21) (2022) 13334–13348.
[5] D.-H. Xie, P.-C. Guo, K.-Q. Zhong, G.-P. Sheng, Highly dispersed Co/Fe bimetal in carbonaceous cages as heterogeneous Fenton nanocatalysts for enhanced sulfamethoxazole degradation, Appl. Catal. B-Environ. 319 (2022), 121923.
[6] H. Zhang, L. Li, N. Chen, H. Ben, G. Zhan, H. Sun, Q. Li, J. Sun, L. Zhang, Hydroxylamine enables rapid heterogeneous-homogeneous coupled Fenton sulfamethazine degradation on ferric phosphate, Appl. Catal. B-Environ. 312 (2022), 121410.
[7] Z. Yang, C. Shan, J.J. Pignatello, B. Pan, Mn(II) acceleration of the picolinic acid-assisted Fenton reaction: new insight into the role of manganese in homogeneous Fenton AOPs, Environ. Sci. Technol. 56 (10) (2022) 6621–6630.
[8] J. Ma, W. Song, C. Chen, W. Ma, J. Zhao, Y. Tang, Fenton degradation of organic compounds promoted by dyes under visible irradiation, Environ. Sci. Technol. 39 (15) (2005) 5810–5815.
[9] Y. Zhu, R. Zhu, Y. Xi, J. Zhu, G. Zhu, H. He, Strategies for enhancing the heterogeneous Fenton catalytic reactivity: a review, Appl. Catal. B-Environ. 255 (2019), 117739.
[10] X. Cui, W. Li, P. Ryabchuk, K. Junge, M. Beller, Bridging homogeneous and heterogeneous catalysis by heterogeneous single-metal-site catalysts, Nat. Catal. 1 (6) (2018) 385–397.
[11] F. Chen, X.L. Wu, C. Shi, H. Lin, J. Chen, Y. Shi, S. Wang, X. Duan, Molecular engineering toward pyrrolic N-rich M-N_4 (M= Cr, Mn, Fe, Co, Cu) single-atom sites for enhanced heterogeneous Fenton-like reaction, Adv. Funct. Mater. 31 (13) (2021), 2007877.
[12] L.-C. Wang, L.-C. Chang, W.-Q. Chen, Y.-H. Chien, P.-Y. Chang, C.-W. Pao, Y.-F. Liu, H.-S. Sheu, W.-P. Su, C.-H. Yeh, Atomically dispersed golds on degradable zero-valent copper nanocubes augment oxygen driven Fenton-like reaction for effective orthotopic tumor therapy, Nat. Commun. 13 (1) (2022) 1–17.
[13] X. Nie, G. Li, S. Li, Y. Luo, W. Luo, Q. Wan, T. An, Highly efficient adsorption and catalytic degradation of ciprofloxacin by a novel heterogeneous Fenton catalyst of hexapod-like pyrite nanosheets mineral clusters, Appl. Catal. B-Environ. 300 (2022), 120734.
[14] L. Lu, H. Zheng, Y. Li, Y. Zhou, B. Fang, Ligand-free synthesis of noble metal nanocatalysts for electrocatalysis, Chem. Eng. J. 451 (2023), 138668.
[15] X. Hou, X. Huang, F. Jia, Z. Ai, J. Zhao, L. Zhang, Hydroxylamine promoted goethite surface Fenton degradation of organic pollutants, Environ. Sci. Technol. 51 (9) (2017) 5118–5126.
[16] H. Sun, G. Xie, D. He, L. Zhang, Ascorbic acid promoted magnetite Fenton degradation of alachlor: mechanistic insights and kinetic modeling, Appl. Catal. B-Environ. 267 (2020), 118383.
[17] T. Zhang, Y. Wen, Z. Pan, Y. Kuwahara, K. Mori, H. Yamashita, Y. Zhao, X. Qian, Overcoming acidic H_2O_2/Fe(II/III) redox-induced low H_2O_2 utilization efficiency by carbon quantum dots Fenton-like catalysis, Environ. Sci. Technol. 56 (4) (2022) 2617–2625.
[18] L. Lu, S. Zou, B. Fang, The critical impacts of ligands on heterogeneous nanocatalysis: a review, ACS Catal. 11 (10) (2021) 6020–6058.
[19] J. Kim, J. Wang, D.C. Ashley, V.K. Sharma, C.-H. Huang, Enhanced degradation of micropollutants in a peracetic acid-Fe(III) system with picolinic acid, Environ. Sci. Technol. 56 (7) (2022) 4437–4446.
[20] A.H. Jenkins, J.W. Medlin, Controlling heterogeneous catalysis with organic monolayers on metal oxides, Acc. Chem. Res. 54 (21) (2021) 4080–4090.
[21] N. Wang, L. Zhu, M. Lei, Y. She, M. Cao, H. Tang, Ligand-induced drastic enhancement of catalytic activity of nano-$BiFeO_3$ for oxidative degradation of bisphenol A, ACS Catal. 1 (10) (2011) 1193–1202.
[22] M. Huang, T. Zhou, X. Wu, J. Mao, Distinguishing homogeneous-heterogeneous degradation of norfloxacin in a photochemical Fenton-like system (Fe_3O_4/UV/oxalate) and the interfacial reaction mechanism, Water Res. 119 (2017) 47–56.
[23] Y. Yin, R. Lv, W. Zhang, J. Lu, Y. Ren, X. Li, L. Lv, M. Hua, B. Pan, Exploring mechanisms of different active species formation in heterogeneous Fenton systems by regulating iron chemical environment, Appl. Catal. B-Environ. 295 (2021), 120282.
[24] L. Lyu, L. Zhang, Q. Wang, Y. Nie, C. Hu, Enhanced Fenton catalytic efficiency of γ-Cu-Al_2O_3 by σ-Cu^{2+}-ligand complexes from aromatic pollutant degradation, Environ. Sci. Technol. 49 (14) (2015) 8639–8647.
[25] Z. Xie, J. Zhou, J. Wang, C.P. François-Xavier, T. Wintgens, Novel Fenton-like catalyst γ-Cu-Al_2O_3-$Bi_{12}O_{15}Cl_6$ with electron-poor Cu centre and electron-rich Bi centre for enhancement of phenolic compounds degradation and H_2O_2 utilization: the synergistic effects of σ-Cu-ligand, dual-reaction centres and oxygen vacancies, Appl. Catal. B-Environ. 253 (2019) 28–40.
[26] W. Xie, P. Zhang, W. Liao, M. Tong, S. Yuan, Ligand-enhanced electron utilization for trichloroethylene degradation by·OH during sediment oxygenation, Environ. Sci. Technol. 55 (10) (2021) 7044–7051.
[27] J. He, X. Yang, B. Men, L. Yu, D. Wang, EDTA enhanced heterogeneous Fenton oxidation of dimethyl phthalate catalyzed by Fe_3O_4: kinetics and interface mechanism, J. Mol. Catal. A: Chem. 408 (2015) 179–188.
[28] W. Luo, L. Zhu, N. Wang, H. Tang, M. Cao, Y. She, Efficient removal of organic pollutants with magnetic nanoscaled $BiFeO_3$ as a reusable heterogeneous Fenton-like catalyst, Environ. Sci. Technol. 44 (5) (2010) 1786–1791.
[29] M.H. Kastvig, J.P. Bøtker, G. Ge, M.L. Andersen, Measurement of hydrogen peroxide vapor in powders with potassium titanium oxide oxalate loaded cellulose pellets as probes, MethodsX 8 (2021), 101405.
[30] Y. Chen, C.J. Miller, R.N. Collins, T.D. Waite, Key considerations when assessing novel Fenton catalysts: iron oxychloride (FeOCl) as a case study, Environ. Sci. Technol. 55 (19) (2021) 13317–13325.
[31] P. Zhou, W. Ren, G. Nie, X. Li, X. Duan, Y. Zhang, S. Wang, Fast and long-lasting iron(III) reduction by boron toward green and accelerated fenton, Chem., Angew. Chem. Int. Ed. 59 (38) (2020) 16517–16526.
[32] J.P. Perdew, K. Burke, M. Ernzerhof, Generalized gradient approximation made simple, Phys. Rev. Lett. 77 (18) (1996) 3865.
[33] K.S. Sing, Reporting physisorption data for gas/solid systems with special reference to the determination of surface area and porosity (Recommendations 1984), Pure Appl. Chem. 57 (4) (1985) 603–619.
[34] R. Gupta, J. Shah, S. Chaudhary, S. Singh, R.K. Kotnala, Magnetoelectric coupling-induced anisotropy in multiferroic nanocomposite (1-x)$BiFeO_3$-x$BaTiO_3$, J. Nanopart. Res. 15 (10) (2013) 1–9.
[35] M. Huang, Y. Han, W. Xiang, D. Zhong, C. Wang, T. Zhou, X. Wu, J. Mao, In situ-formed phenoxyl radical on the CuO surface triggers efficient persulfate activation for phenol degradation, Environ. Sci. Technol. 55 (22) (2021) 15361–15370.
[36] X. Xue, K. Hanna, C. Despas, F. Wu, N. Deng, Effect of chelating agent on the oxidation rate of PCP in the magnetite/H_2O_2 system at neutral pH, J. Mol. Catal. A: Chem. 311 (1–2) (2009) 29–35.
[37] A.Q.K. Nguyen, Y.-Y. Ahn, G. Shin, Y. Cho, J. Lim, K. Kim, J. Kim, Degradation of organic compounds through both radical and nonradical activation of peroxymonosulfate using $CoWO_4$ catalysts, Appl. Catal. B-Environ. 324 (2023), 122266.
[38] M. Huang, Y. Han, W. Xiang, C. Wang, J. Mao, T. Zhou, X. Wu, H.-Q. Yu, Catalytic oxygen activation over the defective CuO nanoparticles for ultrafast dehalogenation, ACS Appl. Mater. Interfaces 14 (26) (2022) 29964–29973.
[39] J. Xiao, J. Rabeah, J. Yang, Y. Xie, H. Cao, A. Brückner, Fast electron transfer and •OH formation: Key features for high activity in visible-light-driven ozonation with C_3N_4 catalysts, ACS Catal. 7 (9) (2017) 6198–6206.

[40] C. Tai, J.-F. Peng, J.-F. Liu, G.-B. Jiang, H. Zou, Determination of hydroxyl radicals in advanced oxidation processes with dimethyl sulfoxide trapping and liquid chromatography, Anal. Chim. Acta 527 (1) (2004) 73–80.
[41] W.P. Kwan, B.M. Voelker, Decomposition of hydrogen peroxide and organic compounds in the presence of dissolved iron and ferrihydrite, Environ. Sci. Technol. 36 (7) (2002) 1467–1476.
[42] Y. Chen, C.J. Miller, T.D. Waite, Heterogeneous Fenton chemistry revisited: mechanistic insights from ferrihydrite-mediated oxidation of formate and oxalate, Environ. Sci. Technol. 55 (21) (2021) 14414–14425.
[43] J. Zhang, D. Wang, F. Zhao, J. Feng, H. Feng, J. Luo, W. Tang, Ferrate modified carbon felt as excellent heterogeneous electro-Fenton cathode for chloramphenicol degradation, Water Res. 227 (2022), 119324.
[44] H. Fu, J. Wei, G. Chen, M. Xu, J. Liu, J. Zhang, K. Li, Q. Xu, Y. Zou, W.-X. Zhang, S. Xi, X. Chen, S. Li, L. Ling, Axial coordination tuning Fe single-atom catalysts for boosting H_2O_2 activation, Appl. Catal. B-Environ. 321 (2023), 122012.
[45] Q. Zeng, H. Dong, X. Wang, Effect of ligands on the production of oxidants from oxygenation of reduced Fe-bearing clay mineral nontronite, Geochim. Cosmochim. Acta 251 (2019) 136–156.
[46] A.M. Jones, P.J. Griffin, T.D. Waite, Ferrous iron oxidation by molecular oxygen under acidic conditions: the effect of citrate, EDTA and fulvic acid, Geochim. Cosmochim. Acta 160 (2015) 117–131.
[47] P. Zhang, S. Yuan, Production of hydroxyl radicals from abiotic oxidation of pyrite by oxygen under circumneutral conditions in the presence of low-molecular-weight organic acids, Geochim. Cosmochim. Acta 218 (2017) 153–166.
[48] C.E. Noradoun, I.F. Cheng, EDTA degradation induced by oxygen activation in a zerovalent iron/air/water system, Environ. Sci. Technol. 39 (18) (2005) 7158–7163.
[49] D.W. King, H.A. Lounsbury, F.J. Millero, Rates and mechanism of Fe(II) oxidation at nanomolar total iron concentrations, Environ. Sci. Technol. 29 (3) (1995) 818–824.